Journal of Applied Geophysics 230 (2024) 105527

Contents lists available at ScienceDirect

Journal of Applied Geophysics

journal homepage: www.elsevier.com/locate/jappgeo

# Electrical resistivity tomography: A reliable tool to monitor the efficiency of different irrigation systems in horticulture field

Agnese Innocenti [a,b,*], Veronica Pazzi [b], Marco Napoli [a], Rossano Ciampalini [b], Simone Orlandini [a], Riccardo Fanti [b]

[a] Department of Agriculture, Food, Environment and Forestry, University of Firenze, Firenze 50144, Italy
[b] Department of Earth Sciences, Univeristy of Firenze, Firenze 50121, Italy

ARTICLE INFO

*Keywords:*
ERT
Drip irrigation
Soil moisture
Water management
Ridge plastic film

ABSTRACT

Water management in agricultural systems is essential for optimal crop yields without incurring excessive water costs and wastage. The choice of irrigation method is crucial for better water management and distribution. The drip system appears to be among the best methods in the field of precision agriculture. In addition to the irrigation system, mulching with ridge plastic film to drain excess water is widely used to increase crop yields in terms of plant water availability. In this study, the time-lapse Electrical Resistivity Tomography (ERT), a not-invasive geophysical technique, is proposed as a simple and reliable method to evaluate the effectiveness of the irrigation systems and to monitor the changes in water content over time and over a volume of soil. ERTs data were compared to moisture ones retrieved from sensors that record continuously over time, but punctually. The ERT investigations were conducted in melon-growing lands in southern Tuscany (Italy). Measurements were carried out on two different fields in two periods: spring and summer. The aim of the work was to evaluate, by means of volumetric measures of the soil conductivity, the effectiveness of three different drip systems and of the mulch ridge. In both the monitored fields the ridge was created in a half portion of the field itself, while the other part of the land was left plat. Geoelectrical investigations associated with humidity sensors have shown that in the summer a too high mulch ridge quickly drains the irrigation water, bringing the root zone into a water deficit. The ERTs also provided good results relating to the irrigation system, demonstrating that a three-lines drip irrigation system, compared to a two-lines one, manages to distribute the irrigation water homogeneously, guaranteeing a constant water content for the plants over time.

## 1. Introduction

Water plays a key role in agricultural production (Chartzoulakis and Bertaki, 2015). Irrigated agricultural soils account for about 20 % of cultivated land (Wanniarachchi and Sarukkalige, 2022). However, water management in agriculture is becoming an increasingly actual issue in a period of severe climate changing. Climate change can lead to adverse effects on agricultural production in many parts of the world (Liu et al., 2022). Not only in terms of water scarcity but also in terms of managing the frequent water bombs the world is increasingly witnessing, that lead to flooding fields and ruining crops. Sustainable management of water for irrigation aims at finding the optimal balance between availability, water needs in terms of quality, quantity, and cost (Chartzoulakis and Bertaki, 2015).

The pursuit of sustainability and water demand management requires adequate knowledge of soil water availability during the growth phase of the crop and also the water storage capacity of the soil (Chartzoulakis and Bertaki, 2015; Borsato et al., 2020; Ratke et al., 2023). As part of increased and more informed water resource management, researchers and farmers have paid special attention to irrigation scheduling, i.e., when and how much to irrigate. However, the optimal time for irrigation is related to different parameters such as crop growth, water stress, and water availability. Consequently, the method of irrigation, i.e., the way to put water into the agricultural soil, cannot be neglected (Chartzoulakis and Bertaki, 2015; Gu et al., 2020; Pereira et al., 2020; Bwambale et al., 2022).

The drip irrigation method is among the most widely used and most effective for water management in agriculture (Arshad, 2020; Zhang et al., 2022). For proper functionality of the drip system, it is necessary to know the environmental, the climatic conditions, and the type of crop

* Correponding author at: Department of Agriculture, Food, Environment and Forestry, University of Firenze, Firenze 50144, Italy.
*E-mail address:* agnese.innocenti@unifi.it (A. Innocenti).

https://doi.org/10.1016/j.jappgeo.2024.105527
Received 6 March 2024; Received in revised form 22 September 2024; Accepted 25 September 2024
Available online 3 October 2024

where the system is applied. Correct planning of such a system is to be considered necessary and essential to ensure its maximum efficiency in the use of the water available and, above all, to make it available to the plants in the greatest possible quantity, avoiding waste (Arshad, 2020; Shi et al., 2022).

Another method often associated with the drip irrigation system in horticulture is the film mulching ridge. This system prevents water loss through spraying and improves soil surface temperature. Mulching with plastic film can, in fact, improve the hydrothermal conditions of the soil surface, optimising crop yield (Zhang et al., 2022). As reported in Zhou and Dahlin (2003) the mulching film limits the evapotranspiration of water from the soil and due to the effect of capillarity, the water moves to the upper layers ensuring stable water content. It also ensures good moisture and water content near the plant. The increase in temperature, on the other hand, is enabled by solar energy passing through the film, which heats the air and soil underneath, creating a greenhouse effect (Wang et al., 2005). The mulch ridge performs the function of water regulation in horizontally lying land. This is an agronomic practice adopted in the plains and has the aim of maintaining the minimum thickness of the surface layer of the soil, which must be free from percolating water, so that the normal development of the plant can be guaranteed (Li et al., 2023). The mulch ridge is created where surface drainage is not installed and allows the water table to be lowered in order to prevent the appearance of surface water stagnation, encouraging the flow of water towards collection ditches generally positioned along the edges of the field. The ridge consists of creating a convex profile of the soil surface through specific plowing. The slope of the ridge depends on the type of terrain, generally in the range 1–3 % (Berger et al., 2013; Gao et al., 2019; Liu et al., 2020; Luo et al., 2023).

The correct management of the drip system in a horticultural context where film mulching is used, requires a good knowledge of the volumetric water content (VWC) in the soil. VWC is a parameter that can be measured using soil humidity sensors. It can provide indications on the water content and it can help understanding how the irrigation water is distributed in the soil, thus making it possible to better schedule irrigation while avoiding waste (Ratke et al., 2023). However, these sensors are point humidity monitoring systems, that means they provide information limited to a single point in the subsoil. They do not allow a view of the water content in areal terms.

The goals of this study was to evaluate the effectiveness of the two- and three-drip irrigation system associated with the mulch cover in two different climatic seasons (spring and summer). To do that, data obtained by means of full 3D Electrical Resistivity Tomographies (ERT) and humidity sensors were compared. ERT is a non-invasive geophysical method capable of estimating the spatial and temporal variation of soil conductivity by measuring the electrical potential differences at different points on the ground surface. (Loke, 2004; Allred et al., 2008; Blanchy et al., 2020). In general, geophysical techniques are indirect non-destructive investigation methods that allow to reconstruct a subsoil model in terms of layers and materials based on measurements of the physical parameters of the ground. In particular, agricultural geophysical investigations are used to characterize the first meter of soil, which includes the crop root zone, and to investigate soil profiles (Allred et al., 2008; Blanchy et al., 2020). ERT method allows to cover a wider area than traditional humidity sensors, and conductivity has found to be a useful proxy for: a) the water content and soil moisture (Brunet et al., 2010; Beff et al., 2013; Alamry et al., 2017; Vanella et al., 2022), b) the soil-root interaction (Cassiani et al., 2015; Vanella et al., 2018; Mary et al., 2019), c) the salinity (Callaghan et al., 2017; Brindt et al., 2019; De Carlo et al., 2020), and d) the soil texture (Blanchy et al., 2020).

In Section 2 the study area is described, while in Section 3 the methodological approach and the experimental set-up are presented. Section 4 summarizes the results that are discussed in Section 5. The final remarks are illustraded in Section 6.

## 2. Study site

The survey campaign was carried out in an agricultural field used for the cultivation of melons (*Cucumis melo*) in Barbaruta (42.804113° N, 11.02322° E; 19 m above sea level) in the municipality of Braccagni (Grosseto, Tuscany - Italy, Fig. 1). To achieve the specific goals mentioned in Section 1, the high-resolution 3D-ERTs were acquired in two different fields (marked in red in Fig. 1) and in two different melon growing periods (April–June 2023 and June–August 2023).

The investigation site is characterized by soils with low-moderate sodicity. The geology of the area is made up of Holocene coastal lagoon deposits (https://regione.toscana.it/geoscopio/geologia.html). The soil (Fig. S1 in the Supplementary Material Section) is classified as Calcaric Vertisol under the WRB reference (Mantel et al., 2023) and has a sequence Ap1/Ap2/$Bgs_1$/$Bgs_2$, it is alkaline, with a generalized clay texture and absence of skeleton. The Ap horizons (0-46 cm) are massive, humid, especially in their lower part (40-45 cm). In the deep horizons ($Bgs_1$,$Bgs_2$; 46–120 cm) were found redoximorphic features, a weak medium wedge structure, shrink-swell cracks, and the presence of slicken-sides. Moderate sodicity is observed in the *Bgs* horizons. The occurrence of a surface crust of about 3 cm with lamellar structure, dry, overlying a sealed layer of medium subangular aggregates, reveals a weak structure stability of the topsoil aggregates.

## 3. Methodological approach and experimental set-up

### 3.1. ERT acquisitions

As mentioned in the Introduction, the ERT technique is able to show the spatial and temporal variation of soil resistivity (or its inverse, i.e., the conductivity). This technique aims at characterize these changes at various depths by means of current and potential measurements on the surface (Patrizi et al., 2022). Every material on Earth, including rock and soil, has in fact an intrinsic property called resistivity, which depends on the relationship between current density and the electric potential gradient (Loke, 2004). The resistivity of soil is influenced by its composition, water content, and temperature. Water, due to its composition, conducts very well, which is why a soil rich in water is defined as a good conductor of current. This is why geoelectrics is used to locate water tables (Light et al., 2004; Vanella et al., 2021; Acosta et al., 2022.

ERT technique is based on the injection of an electrical current in the subsoil by means of applying a voltage difference to a two source electrodes (usually called current electrodes) and by measuring the subsoil voltage at another pair of electrodes (usually called potential electrodes). To collect current and voltage data the four electrodes are commonly arranged on the surface according to different layouts (Dahlin, 2000; Zhou and Dahlin, 2003). The result is the measure of the apparent resistivity, that can be converts in real resistivity solving the inverse modeling problem (Loke, 2004; Vanella et al., 2022). An instrument connected to numerous electrodes (usually the minimum number is 24) allows to automatically select the four electrode at each measurement and to acquire current and voltage values to obtain the apparent resistivity which has to be converted into real resistivity by solving the inverse modeling problem (Patrizi et al., 2022; Vanella et al., 2022). The final result will be a color image, where the various colors represent the different subsurface resistivity/conductivity values (Li et al., 2020).

Data were collected using a 10-channel SyscalPro receiver from Iris (Orléans, France), which allowed the use of 72 electrodes arranged on 3 parallel lines for full 3D data acquisition. Full 3D data acquisition means that the entire volume of soil is investigated and not just the portion below the electrodes because the quadripoles are both in-line (the Tx and Rx dipoles are arranged along the electrode line and thus the acquired apparent resistivity value lies below the electrode line) and cross-line (the Tx and Rx dipoles belong to two different electrode lines and


**Fig. 1.** a) Location of the study area near Grosseto (Tuscany, Italy; b) photo of the melon fields; c) black rectangles indicate the melon field object of the present study.

thus the acquired apparent resistivity value lies between the electrode lines). Three 3D-experimental set-up were arranged in two different areas of the field (marked in black in Fig. 1c), for a total of 6 acquisition layout. The electrode set up used was optimized during a campaign in summer 2021 and used for investigation on the irrigation system during summer 2022. The results of the 2022 campaign are described in detail in Innocenti et al. (2024). Specifically, each layout is made of 72 surface electrodes arranged in three parallel lines of 24 electrodes each. Electrodes are AISI 316 stainless steel bars, 0.20 m long and with a diameter of 5 mm. Each electrode was driven into the ground for approximately half of its length with spacing of 0.30 m between each electrode and each line, reaching an investigation depth of approximately 1.20 m.

Given that each day of survey 6 different ERTs have to be acquired, and considering that a full 3D acquisition using the dipole-dipole (DD) electrode configuration with reciprocal data would have required 1.5 h, an optimized sequence of 2973 data were collected. The sequence was optimized acquiring for each plot a full 3D dataset with reciprocal, creating from it different sub-sets of data, and inverting all of them. Then, comparing the results, it was observed that the quality of the inversion was not affected even if the reciprocal data were not acquired.

The input voltage was 800 V, the number of stacks for each quadripole was set from a minimum of 2 to a maximum of 5 and the quality factor q of each measure (i.e., its standard deviation) was set equal to 2 %. The acquired data were pre-processed and inverted using the commercial software ErtLab (Geostudi Astier S.r.l., Multi-Phase Technologies LLC) (Balasco et al., 2022). The software eliminates outliers, calculates the frequency distribution of various parameters such as voltage, current intensity, geometric factor and apparent resistivity. Through statistical analysis of the data, the removal of the extremes of the tails of each distribution is performed. It also implements Occam's regularisation to optimise the results (Santarato et al., 2011; Pazzi et al., 2018). All ERT data sets were inverted with a noise value of 5 % and achieved convergence. For each dataset, a percentage of data ranging between 1 % to 3 % was removed with a maximum number of 7 iterations to reach convergence.

The implemented layout can be defined as a small-scale ERTs as many in literature (Verdet et al., 2018; Ochs and Klitzsch, 2020), i.e., a high-resolution ERTs, in which the target is very close to the surface and the electrode spacing is therefore in the centimetre or decimetre range. In small-scale ERT the electrode length embedded in the soil (the so called active electrode) has to be lower than the half of the electrode distance (Verdet et al., 2018; Ochs and Klitzsch, 2020). In fact, in the case of small-scale ERT surveys, the electrodes cannot be considered as points but their actual geometry must be taken into account. Thus, in this study, to avoid errors induced by the experimental set up, the electrodes were inserted in the soil up to 10 cm in accordance with Ciani et al. (2024).

The difference between the 3 layout in each area is the drip irrigation system. One was set up with a 2-wing drip irrigation system (BRA2a at the top of Fig. 2a) having the capacity to input 4.1 lh/$m^2$, the second was set up with a 3-wing drip irrigation system (BRA3a+, in the middle of Fig. 2a) capable of supplying about 5 lh/$m^2$, and finally the third (BRA3a-, at the bottom of Fig. 2a) was set up in the same way as BRA3a+, but with the same irrigation capacity as BRA2a distributed over 3 wings instead of 2 (Fig. 2a).

The ERT investigations were carried out in Time-Lapse mode, i.e., acquiring data at different times during the cultivation phase, in this case after at least one irrigation cycle. The electrodes in the two monitoring areas (those marked in black in Fig. 1c) were installed in the fields in two different phases (April, 7th 2023 and June,16th 2023) and were then left in the same position until the end of the investigation (July, 6th 2023 for the first field and August, 28th 2023 for the second field) in order to perform 3D-ERT measurement in the same position. During each measurement, the picket-soil contact resistance on the energising electrode pair was checked (Ciani et al., 2024), which remained constant throughout the study period and did not lead to the identification of a variation due to the irrigation phases and the permanence of the picket in the soil. For each layout, a measurement was carried out prior to the transplanting of the melon plants and of the irrigation cycle, defined as measurement at time 0 ($T_0$), in order to know the resistivity values of the soil without the influence of the plants roots and above all of the irrigation water. Overall, 11 ERTs data sets were acquired during the investigation period (4 for the field arranged from April to July and 7 for the field arranged from June to August).

ERT data were processed using the commercial software *ErtLab*$^{TM}$ (Santarato et al., 2011; Viero et al., 2015; Pazzi et al., 2018; Patrizi et al., 2022), which allowed the creation of a cubic mesh with cells of 0.15 m side, equal to half the distance between the electrodes. The investigation area of each layout has a length of 6.9 m and a width of 0.60 m. Each layout was divided into two parts with different heights, the left side, 3

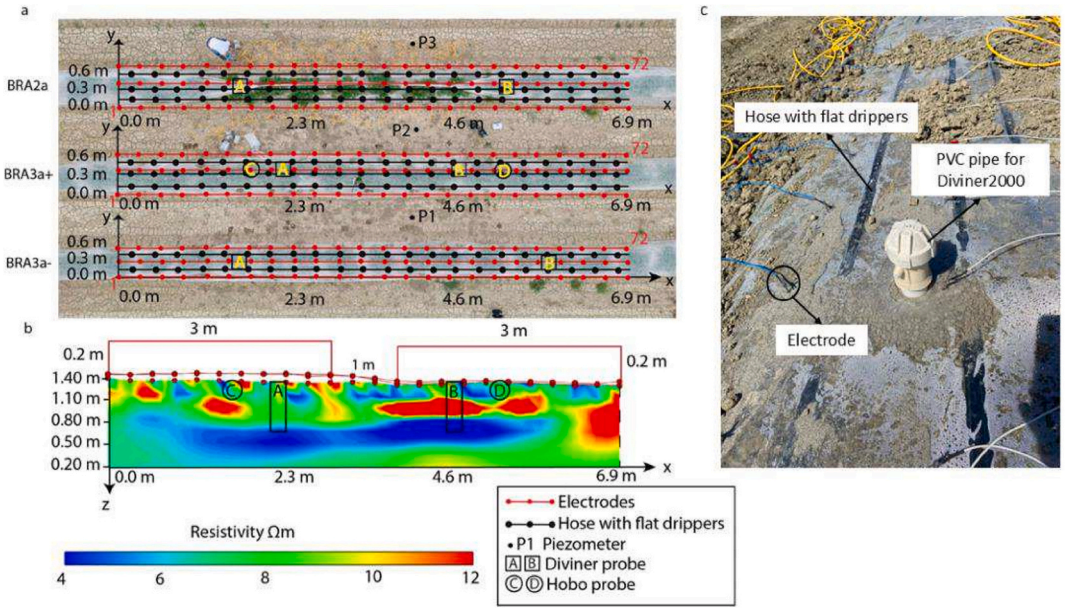


**Fig. 2.** a) Experimental set-up of the study site with the position of the 3 layout (from the top to the bottom: BRA2a, BRA3a+, and BRA3a-), the electrodes (red), the hoses with flat drippers (black), the Diviner2000 sensors (indicated with the square and the letter A and B), the ECH20 10HS sensors (indicated with the circle and the letters C and D), the piezometers (P1, P2, and P3). b) example of electrical tomography and soil profile. c) photo of the ERT profile detail along a row of melons and PVC pipe for Diviner2000 probe. (For interpretation of the references to color in this figure legend, the reader is referred to the web version of this article.)

m long, has a mulch height of approximately 0.20 m, while the right side, 3 m long too, was created at ground level. The transition zone between the area with the ridge and the area without has a length of less than 1 m as visible in Fig. 2b.

### 3.2. Soil moisture acquisitions

In recent years, several techniques have been developed to measure soil moisture. In particular, sensors based on reflectometry (TDR) measurements (Jia et al., 2021). In this work, soil humidity was determined using two sensors: the 10HS Soil Moisture Smart Sensor (produced by HOBO) and the Diviner2000 probe (produced by Sentek Technologies).

The Diviner2000 sensor is a portable and robust probe with a handheld data logging display unit Technologies (2001). It measures the water content in the soil at 0.10 m intervals and uses a portable unit to record data in the field. The sensor must be inserted into an access tube, close to the bottom, to monitor the soil water contents. The tubes used for the Diviner2000 are polyvinyl chloride (PVC) pipes (Jia et al., 2021). The PVC pipes have a length of 0.70 m and a diameter of 5.5 cm. The probe was calibrated before starting the VWC measurements, following the indications of the provider. Two PVC pipes were installed on each layout (indicated with black square and the letters A and B in Fig. 2a), one for the high ridge (A) and one for the portion without the ridge (B), closed at the bottom and at the top with an open cap. The Diviner2000 probe was slid inside these tubes with a constant speed movement during each acquisition campaign.

Two HOBOnet Soil Moisture ECH20 10HS sensors were installed in correspondence with the central plot, indicated with the black circle and the letters C and D in Fig. 2a) and connected to a HOBO® datalogger which records soil humidity and temperature every 30 min. The moisture sensor complements the ECH2O™ 10HS sensor and provides readings directly in volumetric water content (VWC). The probes, having a length of 15 cm, have been installed vertically in the soil, allowing the measurement of soil moisture of 0.001 $m^3$ volume of soil (Innocenti et al., 2024).

Soil resistivity/conductivity is strongly influenced by salinity. In fact, moisture and salinity are inversely proportional to soil resistivity (Cordero-Vázquez et al., 2023). Therefore, both soil moisture and salinity were evaluated in this work in order to carry out a proper analysis of soil resistivity and in order to evaluate whether a leaching effect occurred during the crop cycle due to irrigation. The method adopted to determine salinity is saturated paste extract. The technique consists of collecting soil samples; in this case, samples were collected before the irrigation cycle and at the end of the cycle, that is, at the end of the harvesting phase. It was not possible to collect samples during the growth phase of the melon plants as soil sampling could have caused great disturbance to the plants, also destroying the mulch cloth. Samples were collected manually by using an auger during the installation of the monitoring system, then prior to the transplanting of the melons. The samples were taken at the points indicated with"A" and"B″ (Fig. 2a) for both times of analysis. They were air-dried and sieved to 2 mm. Then, 20 g of soil was mixed with 100 ml of distilled water for 2 h. After the mixing was completed, the samples rested for 2 h and then were filtered by using Whatman filter. The electrical conductivity of the soils was measured using the HANNA handheld conductivity meter sensor model HI 993310. Salinity was then determined from the electrical conductivity value.

## 4. Results

In this section the rainfall data, the moisture measurements and the time-lapse ERTs result will be presented separately for clarity.

### 4.1. Rainfall

The electrical resistivity of a soil is closely related to the moisture and water content present in the soil. In this case, the input of water, and thus the increase in moisture and water content of the soil, may be due to rainfall events and the irrigation cycle. However, while rainwater is (almost) distilled water and therefore has a very high resistivity, irrigation water has a resistivity value that is strictly dependent on its ion content (and type), so a study was conducted on the rainfall that occurred during the investigation period by acquiring rainfall data from the nearest weather station (LAT 42.769 LON 11.016) using the SIR application of the Tuscany Region (https://www.sir.toscana.it). During

the study period between April–June 2023 for the first field and June–August 2023 for the second field, the area was affected by major rainfall events, with total rainfall of 212 mm, of which about 177 mm occurred between April and June, approximately 45 % of the annual precipitation in 2023.

The Fig. 3 shows the rainfall series recorded in the vicinity of the study area in the year 2023; the two light blue rectangles highlight the rainfall events occurred during the field test. In detail, April, May, and June were found to be particularly rainy (light blue). April recorded 13 rainfall events, the largest of which was April, 8th 2023 with 35.4 mm of rain (the day after the Field 1 was installed). May recorded 22 events, with a peak of 17.6 mm on May, 1st 2023. It clearly emerges that the first field was affected by intense rainfall, which affected the electrical conductivity measurements, making it difficult to discriminate the effect of rainwater from that of irrigation water. The survey period for the second field, on the other hand, shows a drier period in terms of rainfall (dark blue rectangle in Fig. 3). From June to August, in fact, only two major rainfall events occurred, one on July, 1st with 22.6 mm and the second on August, 5th with 8.6 mm. The geoelectrical and moisture measurements made during this period were subject to less rainfall, leading to the conclusion that the measured electrical conductivity is a function of the conductivity of the soil itself and the effect of irrigation water.

During the June–August campaign, a system was installed to monitor the effect of irrigation water on the soil, consisting of 3 piezometers 1.5 m long, open at the bottom and sealed at the top to prevent the entry of rainwater (Fig. 2a). Several holes were drilled on all sides of the piezometers to allow irrigation water to enter. During the survey campaign carried out in 2021 (Innocenti et al., 2024), in fact, the ERT results has highlighted a stratification of the soil, in which 3 layers were evident: the upper one representing the mulching ridge, the intermediate one the tilled land, characterized at the base by a layer made waterproof by subsequent tillage of the soil, in which an accumulation of water was observed over time during irrigation cycles. Finally, the deepest one, which represents the layer of untilled soil. The accumulation of water in the second layer (about 30 cm below the ground level) was verified in the June–August 2023 Field 2 campaign thanks to the piezometers which, in this context,identify the depth at which an accumulation of irrigation water occurs, and allow to calibrate the ERTs results.

Table 1 shows the piezometric readings taken with a phreatometer (an instrument that measures the static water level in a well or piezometer). The P2 piezometer on average recorded rather deep values compared to the others (P1 and P3), and as shown later on in this section not always in agreement with what the ERTs show. This is probably caused by the desiccation fractures that occur in heterogeneous silty clay and non-uniformly worked soils, which create horizontal and vertical fracture and consequently lead water flows to concentrate more in certain areas than others (Inoue, 1993; Cabangon and Tuong, 2000; Li et al., 2016; Wang et al., 2018). The influence of rainfall in piezometric readings is almost nil because in the 16 days before the first reading there was only one small rainfall episode (0.2 mm on June, 18th 2023) two days after the installation (occurred on June, 16th 2023). For this reason, a value of 0 was entered at time $T_0$, as no evidence of the water table was found during installation.

**Table 1**
Piezometric readings. P1, P2 and P3 represent the piezometric measurements (see Fig. 2 for location) taken during each campaign.

| Time | P1 [m] | P2 [m] | P3 [m] |
|---|---|---|---|
| $T_0$ | – | – | – |
| $T_1$ | 0.3 | 1.3 | 1.3 |
| $T_2$ | 0.3 | 1.2 | 1.5 |
| $T_3$ | 0.3 | 1.3 | 0.7 |
| $T_4$ | 0.4 | 1.2 | 0.7 |
| $T_5$ | 0.3 | 1.2 | 0.6 |
| $T_6$ | 0.5 | 0.6 | 0.6 |

### 4.2. Moisture measurements

As mentioned in Section 3, moisture measurements were carried out by means of two types of probes, the Soil Moisture ECH20 10HS probe and the Diviner2000 probe. The first one makes continuous measurements, and it made possible to identify which VWC peaks were caused by the rain and which by the irrigation cycle. Fig. 4 shows the graph of VWC recorded in Field 1 and in Field 2 in relation to the rainfall events that occurred during the campaigns. The yellow line represents the VWC value recorded at point C, i.e., on the elevated mulch ridge, and the green line the values measured at point D, i.e., in the area with mulch ridge close to the ground level (see Fig. 2a for the location). From the

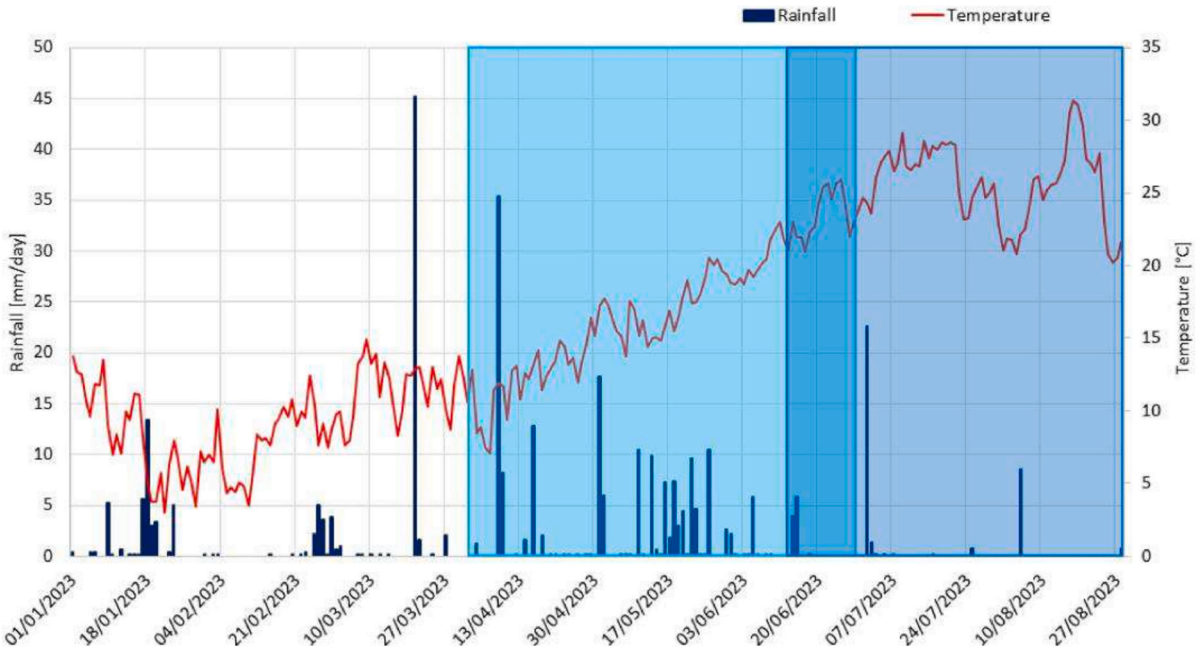


**Fig. 3.** Graph of daily rainfall and average daily temperature for the period between January and August 2023. The light blu rectangle shows the study period of the first field, and the dark blu rectangle shows the period of the second field.

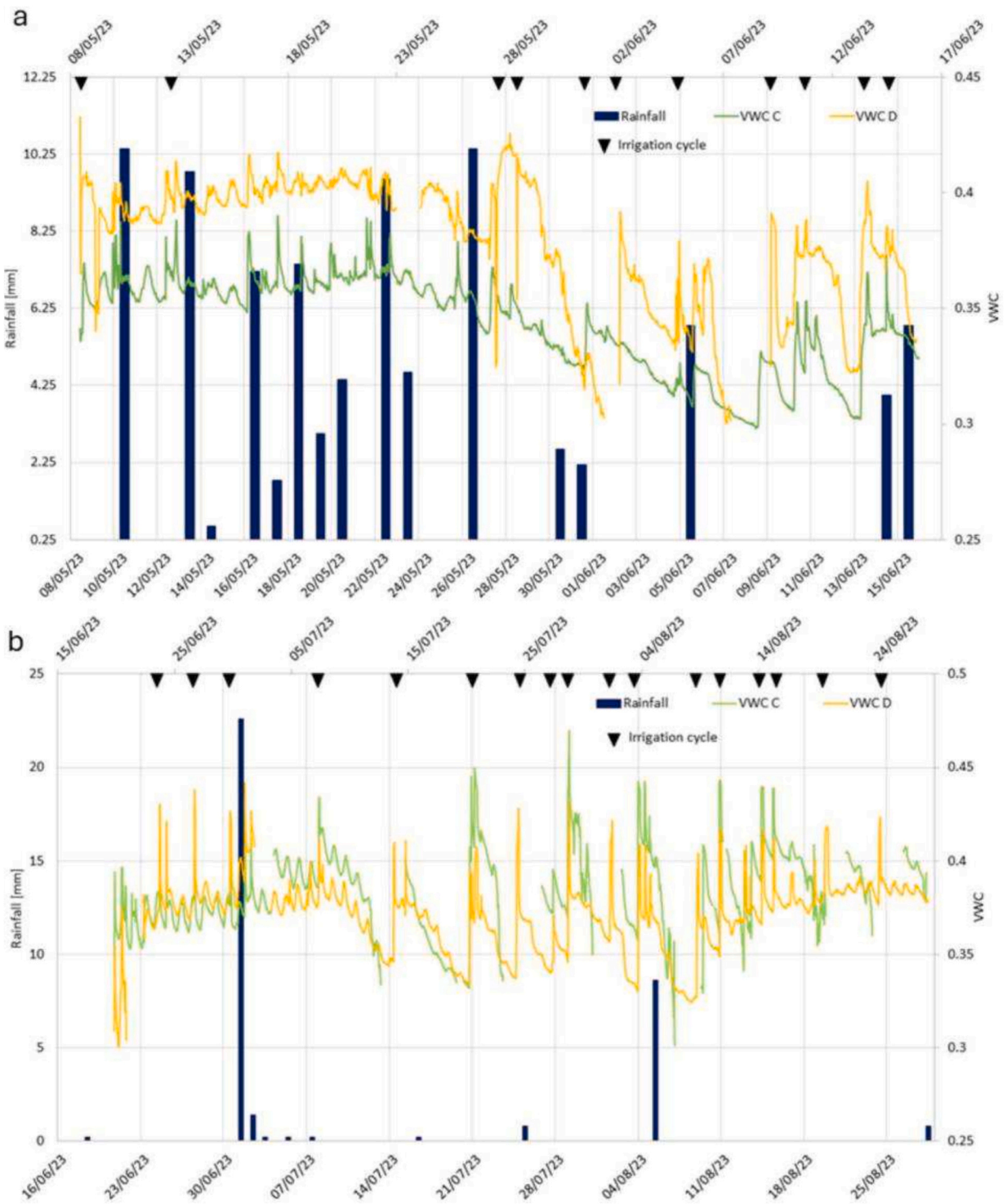


**Fig. 4.** Temporal variation of soil VWC measured by ECH20 10HS sensors and rainfall events for the period a) April–June, and b) June–August. Green curve represents data acquired on the mulch ridge with an elevation of 0.20 m, while yellow curve represents data acquired on the plot with an elevation less of 0.10 m. The black triangles represent the irrigation cycles. (For interpretation of the references to color in this figure legend, the reader is referred to the web version of this article.)

graphs, we can observe the peaks of VWC caused by the rainfall and those, on the other hand, that occurred as a result of the irrigation, generally carried out during the morning for about 2.5 h every two days. Peaks caused by irrigation show a greater extent, recording an immediate increase in VWC followed by a gradual decrease over time. In some periods data are missing because of technical problems in the acquisition system.

The Diviner2000 probe was used to monitor soil water content in each layout. Of the 12 PVC pipes installed for measurement (6 in each field), 3 were not productive in terms of data (one located in layout BRA2a of Field 1 and the other two in layout BRA3a- and layout BRA2a of Field 2), because there was a buildup of water inside the pipe that did not allow the probe to be inserted, and thus data to be acquired. The probe is capable of acquiring a measurement every 10 cm up to a

maximum depth, in this case, of 70 cm. Only data from the Field 2 are presented in this paper (Fig. 5), because measures related to Field 1 are insufficient in number for proper analysis (the data for Field 1 can be found in the Supplementary Material Section in Fig. S2). The data (Fig. 5) show significant variation between the three different irrigation systems and between the two different heights for the depths of 10 cm, 20 cm, and 30 cm, while at a greater depth the data show high water contents for all the three layouts and on both heights. This also confirms the findings of piezometers that show the presence of water from 30 to 40 cm depth. Furthermore, the area of interest for the study is between the surface and a depth of 20 cm, i.e., where there is the maximum root development, so here only the graphs for depths between 10 cm and 40 cm are shown, but in the Supplementary Material also data for the other depth are available (Fig. S3).

Looking at the data (Fig. 5) in terms of difference in VWC between point A (peak height of about 20 cm) and point B (ridge height of about 10 cm) it is clearly visible that point B has higher water content in both BRA3a- and BRA3a + layouts. This is clearly visible up to a depth of 30–40 cm. From a depth of 40 cm, the VWC values for all the three layouts vary between 30 and 45 ($m^3/m^3$), showing very similar values to each other for the levels at 50 cm, 60 cm, and 70 cm depth.

### 4.3. ERTs and soil conductivity

In this section, only the Field 2 ERTs data are presented, as it, been equipped also with piezometer, allows for a more complete discussion than Field 1. In the Supplementary Material Section results for Field 1 are reported (Fig. S4, Fig. S5, Fig. S6, and Fig. S7).

#### 4.3.1. The $T_0$ soil condition

An important consideration to take into account for the interpretation of the results concerns the starting conditions of each layout. The ERTs (Fig. 6), and the VWC values recorded by the Diviner2000 probe at time $T_0$, clearly show that the three layouts of Field 2, the one

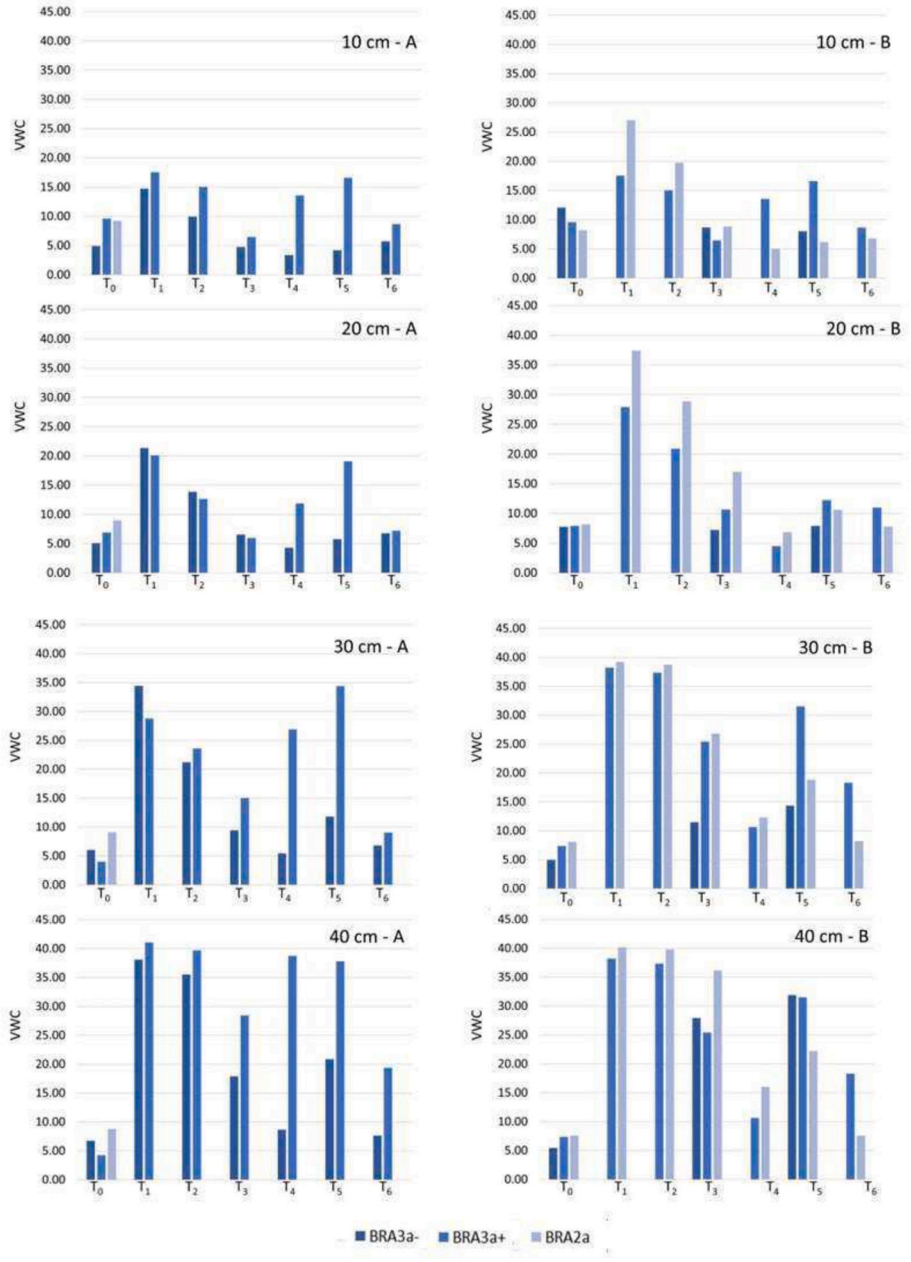


**Fig. 5.** Temporal variation of VWC measured by Diviner2000 sensors at depth of 10 cm, 20 cm, 30 cm and 40 cm, at points A (high ridge) and B (low ridge).

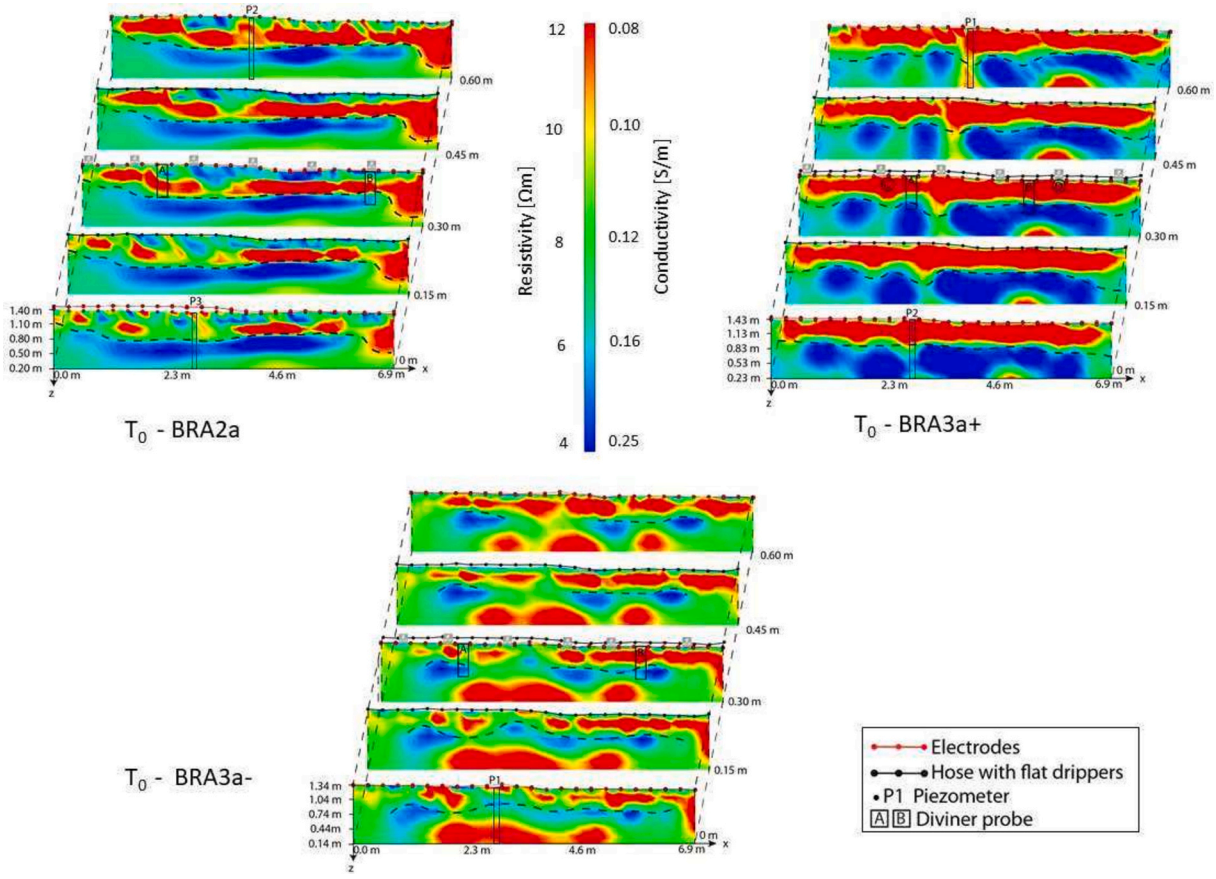


**Fig. 6.** ERT results for BRA3a-, BRA3a+, and BRA2a at time $T_0$. The black dotted line represents the depth of tilled soil at this acquisition time.

investigated from June to August, present rather different characteristics from each other. The tillage of the soil and the creation of the mulch ridge, carried out using machinery in a period (June) characterized by rather anomalous rainfall for the area which made the soil particularly rich in water, led to the creation of non-homogeneous and uniform fields. Consequently, the results of the time-lapse analysis are affected by this initial condition.

### 4.3.2. *Time-lapse ERTs*

The ERTs inversion outputs show significant differences among the three layouts. For brevity, here only three of the six ERTs for each layout carried out are shown (Fig. 7a, Fig. 8a, and Fig. 9a), but in the Supplementary Material also the other data are shown (Fig. S8, Fig. S9, and Fig. S10). Moreover, in Fig. 7b, Fig. 8b, and Fig. 9b the spatial and temporal distribution of water fluxes in terms of pixel by pixel resistivity difference are shown. They were calculated by running the difference between the times $T_1$-$T_0$, $T_3$-$T_1$, and $T_6$-$T_3$. In these figures areas in blue highlight where an increase in conductivity occurred over time, that means water accumulation, while red areas highlight where a decrease in conductivity occurred over time, that can be associated with the water flowing away.

Fig. 7a shows the ERTs results related to the BRA2a layout for times $T_1$, $T_3$, and $T_6$. At times $T_1$ and $T_3$, a clear difference is observed between the high and low ridges, the latter showing higher conductivity values. The distribution of irrigation water is not homogeneous throughout the investigated area. It can be observed, in fact, that the most conductive surfaces (first 10 cm) are concentrated near the drippers compared to the ends of the plot and that in the low ridge the water concentration is higher than in the high peak. In addition, the vertical slice corresponding to 0.60 m on the y-axis is more conductive in all tomographies.

Fig. 8a shows the ERTs results of the BRA3a + layout at times $T_1$, $T_3$, and $T_6$. This layout has the characteristic of having an irrigation system capable of introducing 5 lh/$m^2$. Of all the three systems tested, this one has much higher conductivity values. The difference between point"A" and"B" is much less visible, however it can be noted, in particular at $T_3$ and $T_6$, how the low peak has slightly higher conductivity values than the high peak, where there is a greater concentration of high resistivity areas. These tomographies also show how the distribution of irrigation water is much more homogeneous across the entire area. This irrigation system immediately created an excessive accumulation of water below the root zone, indicated in Fig. 8 with a dotted black line, and also confirmed by the piezometer P1.

Fig. 9a shows the ERTs results of the BRA3a- layout, characterized by an irrigation system having the same capacity as the BRA2a, i.e., 4.1 lh/$m^2$, but distributed by a system with three dripping wings. The images show a good distribution of irrigation water, represented by the conductive zones. Also in this case the most conductive area is the lower ridge. The surface level between 1.04 m and 1.34 m is rather constant over time and the water distribution is much more homogeneous than the BRA2a system despite the quantity of water introduced being the same. The tomographies therefore show that this system offers a better supply of water to the root system, as the downward runoff is also lower than BRA3a + and BRA2a, demonstrating less water waste.

## 5. Discussion

Irrigation management combined with the agricultural production system can influence soil moisture and consequently crop yield (Ratke et al., 2023). Knowing the variation in water content in the root zone is therefore fundamental to understand the filtration mechanism of irrigation water.

Table 2 reports the salinity values determined by the laboratory

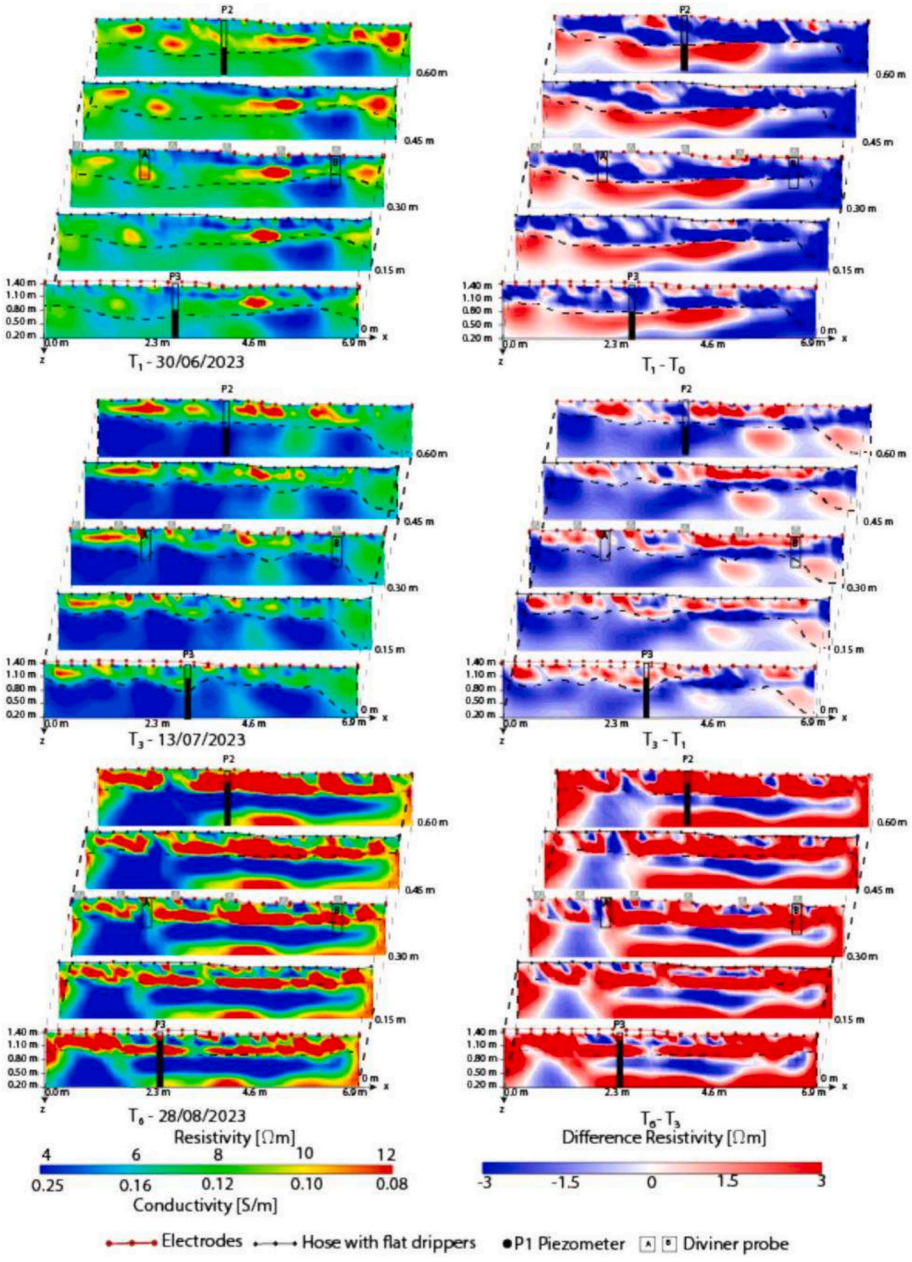


**Fig. 7.** a) Electrical resistivity tomography campaign results of BRA2a at time $T_1$, $T_3$, and $T_6$. The dashed black line represents the level of the water table. b) Changes in resistivity at times $T_1$-$T_0$, $T_3$-$T_1$ and $T_6 - T_3$.

analysis on saturated paste extract, relating to Field 1 and Field 2 and represented in terms of electrical conductivity expressed in mS/cm (Zhang et al., 2005; Cordero-Vázquez et al., 2023; Wang et al., 2023).

The values for the Field 1 show a salinity content that does not vary between the pre-irrigation sample and that one taken at the end. This leads to consider that the measured conductivity values are representative of the physical properties of that soil and can be caused only by the variations in the water content. While the data relating to Field 2 show a decrease in salinity at the end of the irrigation cycle. This effect may actually be due to leaching that occurs from irrigation water. Salinity values were considered in the resistivity calculation, normalizing the measured apparent resistivity ($\rho_a$) values respect the EC measured on the samples.

Fig. 4 shows the variation in water content on the surface: the probe, in fact, records the moisture average in a range between 0 cm and 15 cm depth. The two sensors, therefore, show the variation in VWC at two different heights of the mulch ridge. In Field 1 (Fig. 4a) it appears that the yellow line, i.e., the water content in the low ridge (D) is higher than the value recorded in the high ridge (C, green line). This means that in the period between April and June the low ridge had a higher water content than the high ridge. In the period June–August (Fig. 4b), an opposite effect is observed, i.e., the green line, representing the moisture of point C, is slightly higher than the yellow line. The difference between points C and D is smaller in the second field than in the first. This means that in the first field there is greater drainage at point D, compared to point C, where instead, there is a greater water content and with water peaks of greater intensity. At this point the soil is in fact unable to drain the water present, bringing the soil significantly above the field capacity. This results in the presence of an excessive quantity of water at point D in correspondence with the root zone.

If in the meteorological period of April–June the water content recorded in point C is better, in the summer period (June–August) it is the opposite: the VWC recorded in point D is better than in C. The green line during the irrigation cycle is positioned below above field capacity

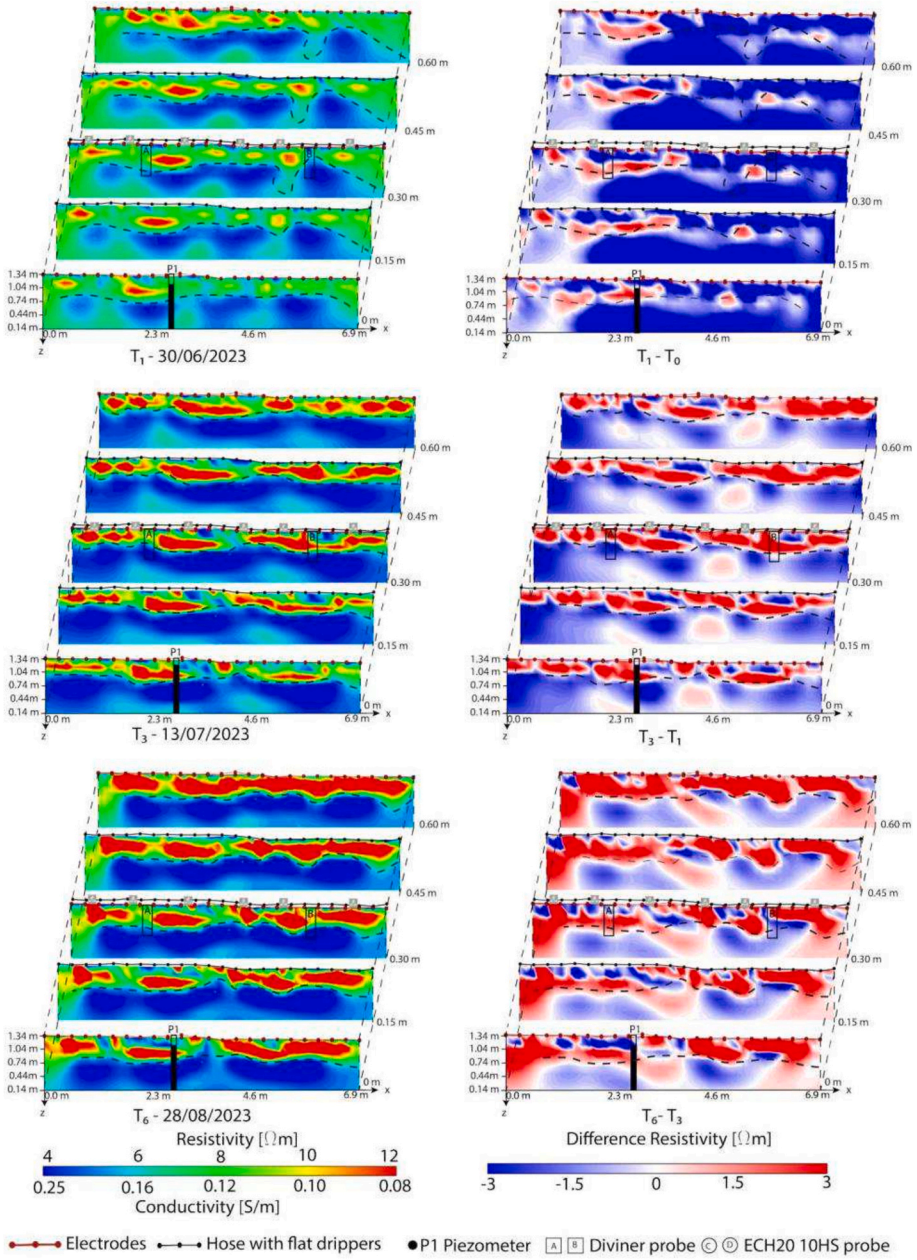


**Fig. 8.** a) Electrical resistivity tomography campaign results of BRA3a + at time $T_1$, $T_3$, and $T_6$. The dashed black line represents the level of the water table. b) Changes in resistivity at times $T_1$-$T_0$, $T_3$-$T_1$and $T_6$ − $T_3$.

(peaks reaching values of 0.45), but during the period between one irrigation and the next, the green line shows excessive drainage (Fig. 4b). This means that the high ridge in the summer period immediately drains the irrigation water to the lower levels, drastically reducing the water content in the root zone, compared to point D where drainage is significantly lower. In fact in this area the pores are able to retain the irrigation water near the roots. Instead, the strong compaction that occurs at point D leads to a large part of the water draining away from the root area.

Layout BRA2a shows very high VWC values compared to BRA3a + and BRA3a- at depths of 10 cm and 20 cm (Fig. 5). Unfortunately, the lack of data on point A for layout BRA2a does not allow further analysis and comparison of that plot with plot BRA3a- which has the same amount of water but distributed over three wings instead of two. However, the data show that over time the water content varies more in plot BRA2a than in BRA3a- and BRA+, leading to the inference of excessive water drainage under the root zone. BRA3a + and BRA3a- show less variation over time, although the paucity of data on BRA3a-"B″ does not allow us to make a greater assessment, but from the available data we might consider the BRA2a system to be insufficient, distributing about 4.1 lh/$m^2$ over a smaller area than BRA3a-.

The higher VWC on BRA2a can be explained by the fact that water is distributed only at the highest part of the ridge, i.e., where the two wings are located and extremely close to the PVC pipe. This allows the Diviner2000 probe to read a higher water content than the same point but on BRA3a-, which manages to distribute the same amount of water over a larger area and consequently leads the probe to read a lower VWC value. In addition, the significant variation in time read on BRA2a compared to BRA3a- can be explained as excessive compaction occurring in the BRA2a system that does not allow water to remain in the root zone but moves rapidly below it. Regarding the BRA3a + layout, the only one on which it was possible to acquire all the data over time, it

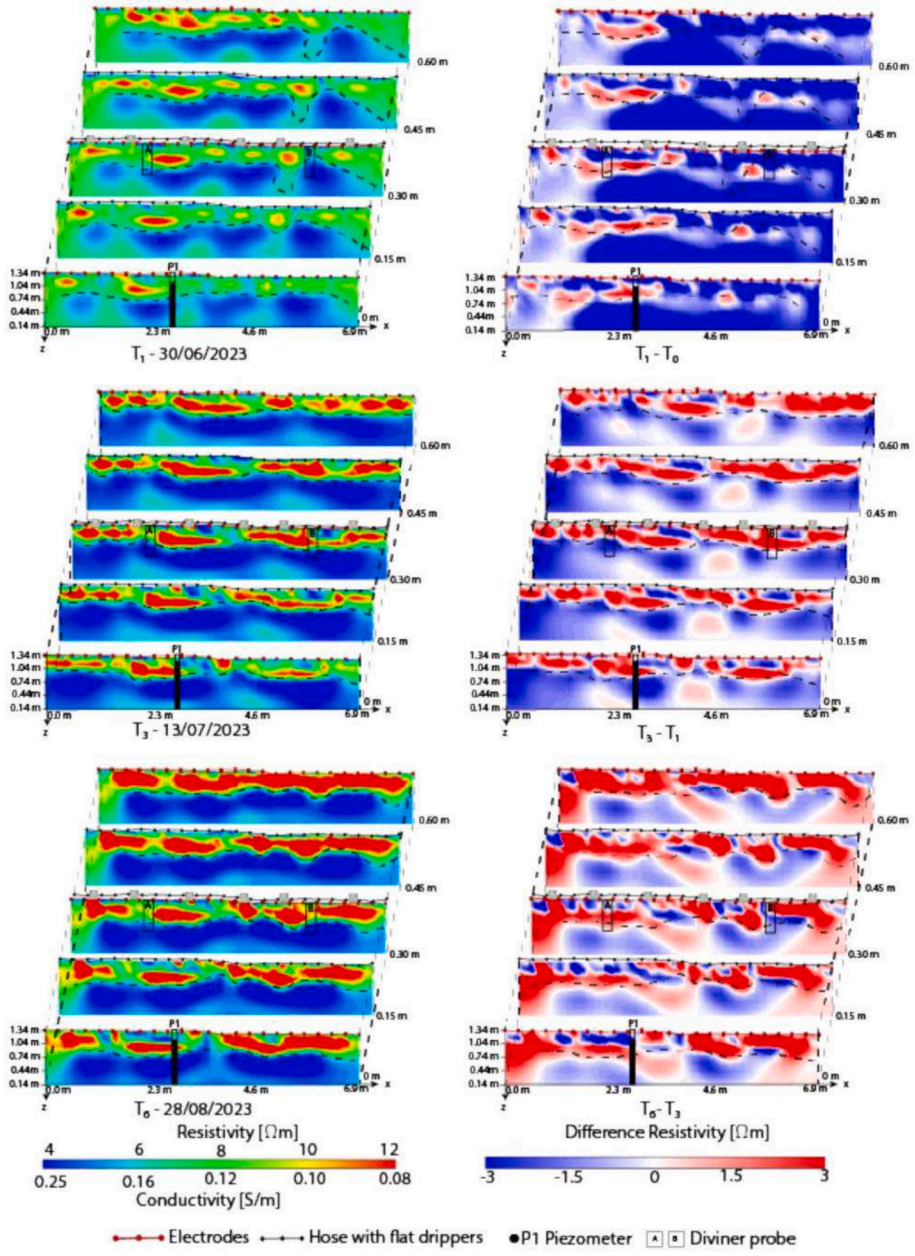


**Fig. 9.** a) Electrical resistivity tomography campaign results of BRA3a- at time $T_1$, $T_3$, and $T_6$. The dashed black line represents the level of the water table. b) Changes in resistivity at times $T_1$-$T_0$, $T_3$-$T_1$and $T_6 - T_3$.

clearly emerges that point B has more water than point A in the root zone, and the variation over time is also lower on B than A. This leads to consider that for the summer period, a ridge height of less than 20 cm is better for roots than a higher ridge. Regarding the amount of water distributed by BRA3a + from the readings taken by Diviner2000 it appears to be excessive, in fact it tends to drain a lot of water in the lower levels, where it is no longer of use to the roots.

Finally, results shown in Fig. 7, confirming what has been observed in the 2022 campaign and that is discussed in a paper currently under review, highlight that the two-line drip system is not able to distribute water evenly over the whole plot. On the contrary, irrigation tends to favor the central area at the expense of the lateral areas and with the passage of time, irrigation water is not retained in the root zone but bypasses this level completely to move to depth where water accumulation occurs as confirmed by piezometer P3. At time $T_6$, the preferential paths of surface water flows are noted, especially at point"A," through which water is able to reach the deep levels.

Results also show that BRA3a + leads to an excessive accumulation of water below the root zone, while BRA3a- offers the better water supply to the root system, causing less water waste.

The best effectiveness and placement of the mulch ridge was by correlating the ERT results with the VWC recorded by the Hobo probe positioned in"C″ and"D″ (Fig. 2a).To evaluate the relationship between electrical conductivity and soil moisture at the two points of interest, VWC data recorded by the ECH20 10HS probe were correlated with electrical conductivity (EC) data. Considering that the humidity sensor records an average value of water content over a depth interval of 15 cm, the conductivity data were obtained by extrapolating from the ERTs output model the average resistivity value relating to the first 15 cm of depth at the point of interest. Fig. 10 shows the relationship between VWC (on the x axis) and EC (on the y axis) for each time starting from $T_1$. It was chosen not to graph the data relating to $T_0$ time as in this phase the ECH20 10HS sensor took more than 24 h to settle down, therefore the VWC value was not reliable. The average VWC was calculated as the

**Table 2**
Salinity values at time $T_0$ and $T_8$ for the first and second field. A and B represent the points of sampling in correspondence of the Diviner2000 sensor.

| Plot Field 1 | ID | EC (mS/cm) $T_0$ | EC (mS/cm) $T_8$ |
|---|---|---|---|
| BRA3a- | A | 0.22 | 0.21 |
| BRA3a- | B | 0.16 | 0.25 |
| BRA3A+ | A | 0.11 | 0.17 |
| BRA3a+ | B | 0.14 | 0.16 |
| BRA2a | A | 0.09 | 0.13 |
| BRA2a | B | 0.10 | 0.18 |

| Plot Field 2 | ID | EC (mS/cm) $T_0$ | EC (mS/cm) $T_8$ |
|---|---|---|---|
| BRA3a- | A | 0.40 | 0.22 |
| BRA3a- | B | 0.38 | 0.12 |
| BRA3a+ | A | 0.24 | 0.16 |
| BRA3a+ | B | 0.32 | 0.15 |
| BRA2a | A | 0.21 | 0.16 |
| BRA2a | B | 0.25 | 0.18 |

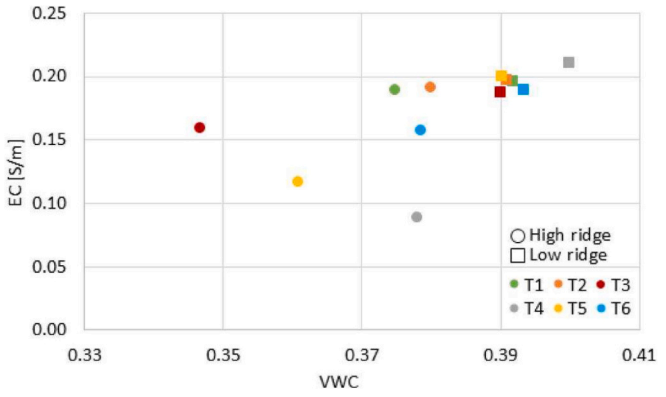


**Fig. 10.** Relationship between the average volumetric water content (VWC), and the electrical conductivity (EC). The circles compare the conductivity and VWC value recorded at point"C", and the squares compare the conductivity and VWC value recorded at point"D". The colors represent acquisition campaigns.

arithmetic mean between the VWC data collected every 30 min during the ERT acquisition. The round and square symbols represent the data purchased on the high ridge and on the low ridge, respectively. The colors, however, represent the acquisition times.

As reported in Araya Vargas et al. (2021), electrical conductivity (EC) is directly proportional to VWC; in fact, as the water content increases, the electrical resistivity decreases, and thus its inverse increases. This is clearly visible in Fig. 10 where at each time the conductivity and VWC increase for the data collected on the low ridge (i.e., for each color that moves from the point to the square). Furthermore, it is observed that data represented by squares present EC and VWC values that are very similar to each other over time. This leads to the deduction that in the low ridge the irrigation water is retained more than in the high ridge, where VWC decreases over time. The decrease in VWC on the high ridge is caused by the fact that the mulch ridge was created with the aim of draining excess water. However, in the summer period, where rainfall is on average lower than in the spring period, the water that is drained is the irrigation water and is consequently removed too quickly from the root zone, putting the plants at greater risk of water stress.

The relation between VWC, recorded by Diviner2000, and EC is shown in Fig. 11 for BRA3a + where data from both the instruments where available for all the times. The left column shows the data for the high ridge, while the right column shows the data for the low ridge. In both representations (histogram and scatter points), a concordance between the two data sets can be observed: when VWC increases, also EC increases, and vice versa. Moreover, it is also to note that the two regression curves are very similar. This was expected, because the correlation between VWC and EC is site specific, and should not depend on the height of the ridge. Using the obtained regression law, it is possible to convert the EC tomographies data into VWC ones, and thus visualize the variation of the water content in the root zone, as shown, as an example, in Fig. 12 for BRA3a + .

This works shows that ERT can be effectively used in agricultural applications as a tool to optimise the irrigation system. However, further developments are needed, e.g., the application of 4D time-lapse inversion instead of a"pixel by pixel variation" as shown in this work. The 4D time-lapse inversion, in fact, allows to emphasize the resistivity/conductivity changes caused by the water infiltration/uptake over time as inversion of all the time-steps dataset, together with constraints along the spatial and temporal dimensions (Karaoulis et al., 2014). Moreover, further developments should concern the definition, thanks to the

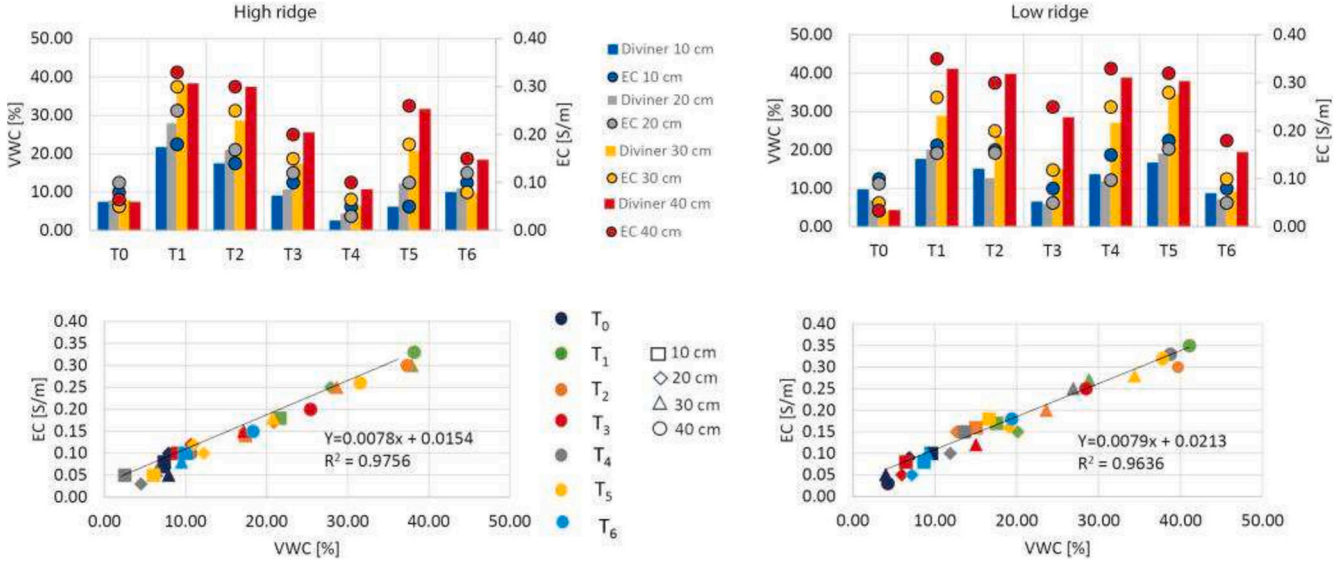


**Fig. 11.** The left column represents the ratio between VWC recorded by the Diviner2000 probe and EC derived from the ERT models for the high ridge. The right column represents the same ratio for the low ridge.

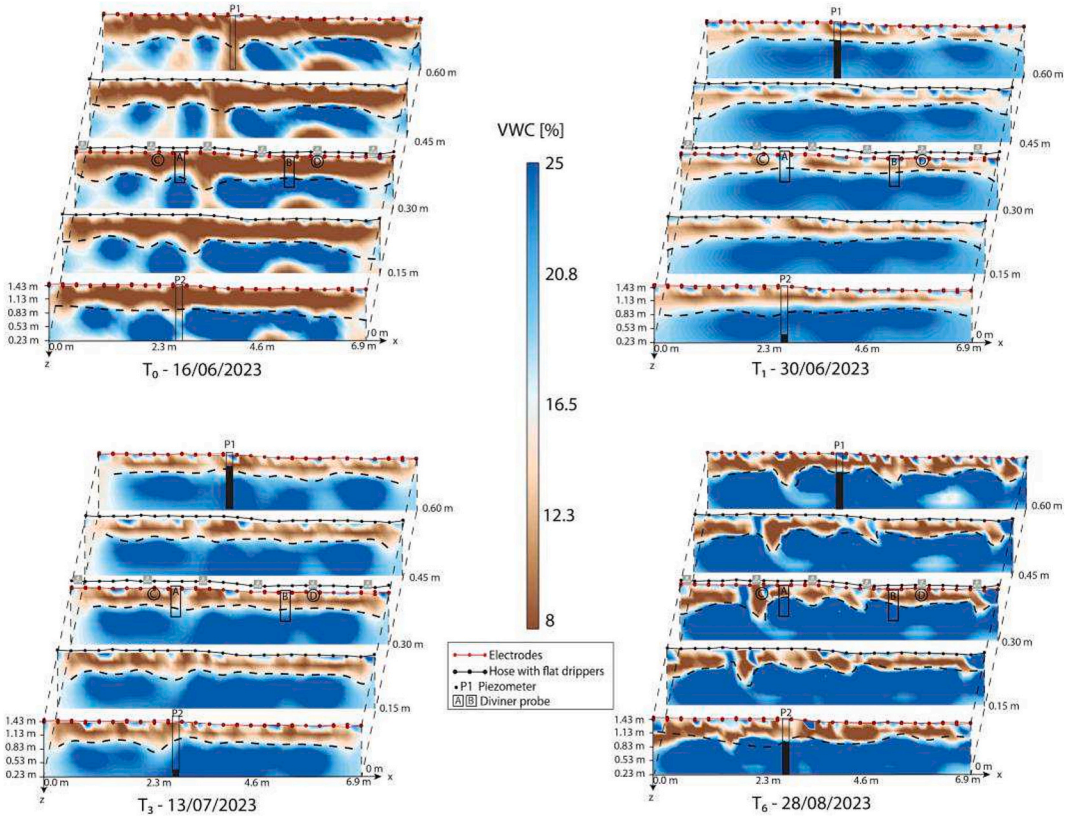


**Fig. 12.** Subsoil VWC distribution in BRA3a + at time $T_0$, $T_1$, $T_3$, and $T_6$. The dashed black line represents the level of the water table.

calibration of laboratory test, of empirical laws to convert electrical resistivity data into water content ones. Finally, the continuous and remotely controlled resistivity/conductivity data acquisition will allow to reduce the time step and better follow the irrigation water flow.

## 6. Conclusions

This study was conducted to evaluate the effectiveness of the two- and three-drip irrigation systems associated with the mulch cover in two different climatic seasons (spring and summer). The soil was particularly rich in clay and was subject to frequent irrigation cycles during melon cultivation. During a previous investigation campaign carried out one year before this study in the same area it emerged that the classic system, i.e., the two-drip lines, was particularly ineffective and that the distribution of irrigation water favored certain areas more than others. Consequently, EC and VWC values had shown a decrease over time in the water content in the root zone and an excessive state of water stress for the plants.

The data collected during the 2023 campaign presented in this study showed the same results for the 2-wing system (BRA2a), while they led to satisfactory results for the BRA3a- (3-wing system and same water flow than BRA2a) and the BRA3a + (3-wing system and highest water flow). In particular, the BRA3a- system has shown that the same quantity of water as the BRA2a distributed over three wings instead of two leads to a greater concentration of water in the root zone over time, slowly draining downwards. On the contrary, the BRA3a + system distributes the water uniformly like the BRA3a- but the quantity introduced was excessive, leading the soil to always be positioned above the field capacity and draining a lot of water downwards. The excessive accumulation of water below the root zone represents a waste of water, as this cannot be used by the root system.

The tests, in addition to considering which system was optimal, also evaluated the effectiveness of the mulch ridge, leading to the deduction that during the spring season a ridge of height equal to or greater than 20 cm is to be considered better than a ridge of less than 20 cm or absent, as it allows excess water, represented by rainfall, to be drained. However, during the summer period, when rainfall is less if not absent, the presence of a much lower ridge (around 10 cm in height) is much more effective as it allows the irrigation water to be retained at the root system avoiding excessive drainage.

## Funding

No research funds have been received.

## CRediT authorship contribution statement

**Agnese Innocenti:** Writing – review & editing, Writing – original draft, Visualization, Methodology, Investigation, Data curation, Conceptualization. **Veronica Pazzi:** Writing – review & editing, Writing – original draft, Visualization, Methodology, Data curation. **Marco Napoli:** Writing – review & editing, Methodology, Investigation, Conceptualization. **Rossano Ciampalini:** Writing – review & editing, Methodology, Investigation. **Simone Orlandini:** Writing – review & editing, Supervision, Project administration, Funding acquisition. **Riccardo Fanti:** Writing – review & editing, Supervision, Project administration, Funding acquisition.

## Declaration of competing interest

The authors declare no competing interests.

## Data availability

Data will be made available on request.

## Acknowledgements

The authors would like to thank O.P. Bristol Soc. Agr. Cons. a r.l. for making the research possible by conducting measurements within their field. Tommaso Concari and his collaborators, Rachele Franceschini and Luca Lombardi for their support during the data collection campaign.

## Appendix A. Supplementary data

Supplementary data to this article can be found online at https://doi.org/10.1016/j.jappgeo.2024.105527.

## References

Acosta, J.A., Gabarrón, M., Martínez-Segura, M., Martínez-Martínez, S., Faz, Á., Pérez-Pastor, A., Gómez-López, M.D., Zornoza, R., 2022. Soil water content prediction using electrical resistivity tomography (ert) in mediterranean tree orchard soils. Sensors 22, 1365.

Alamry, A.S., van der Meijde, M., Noomen, M., Addink, E.A., van Benthem, R., de Jong, S.M., 2017. Spatial and temporal monitoring of soil moisture using surface electrical resistivity tomography in mediterranean soils. Catena 157, 388–396.

Allred, B.J., Ehsani, M.R., Daniels, J.J., 2008. General considerations for geophysical methods applied to agriculture. Handbook Agricult. Geophys. 3–16.

Araya Vargas, J., Gil, P., Meza, F.J., Yáñez, G., Menanno, G., García-Gutiérrez, V., Luque, A., Poblete, F., Figueroa, R., Maringue, J., et al., 2021. Soil electrical resistivity monitoring as a practical tool for evaluating irrigation systems efficiency at the orchard scale: a case study in a vineyard in Central Chile. Irrig. Sci. 39, 123–143.

Arshad, I., 2020. Importance of drip irrigation system installation and management-a review. Psm Biol. Res. 5, 22–29.

Balasco, M., Lapenna, V., Rizzo, E., Telesca, L., 2022. Deep electrical resistivity tomography for geophysical investigations: the state of the art and future directions. Geosciences 12, 438.

Beff, L., Günther, T., Vandoorne, B., Couvreur, V., Javaux, M., 2013. Three-dimensional monitoring of soil water content in a maize field using electrical resistivity tomography. Hydrol. Earth Syst. Sci. 17, 595–609.

Berger, S., Kim, Y., Kettering, J., Gebauer, G., 2013. Plastic mulching in agriculture—friend or foe of n2o emissions? Agric. Ecosyst. Environ. 167, 43–51.

Blanchy, G., Watts, C.W., Richards, J., Bussell, J., Huntenburg, K., Sparkes, D.L., Stalham, M., Hawkesford, M.J., Whalley, W.R., Binley, A., 2020. Time-lapse geophysical assessment of agricultural practices on soil moisture dynamics. Vadose Zone J. 19, e20080.

Borsato, E., Rosa, L., Marinello, F., Tarolli, P., D'Odorico, P., 2020. Weak and strong sustainability of irrigation: a framework for irrigation practices under limited water availability. Front. Sustain. Food Syst. 4, 17.

Brindt, N., Rahav, M., Wallach, R., 2019. Ert and salinity–a method to determine whether ert-detected preferential pathways in brackish water-irrigated soils are water-induced or an artifact of salinity. J. Hydrol. 574, 35–45.

Brunet, P., Clément, R., Bouvier, C., 2010. Monitoring soil water content and deficit using electrical resistivity tomography (ert)–a case study in the cevennes area, France. J. Hydrol. 380, 146–153.

Bwambale, E., Abagale, F.K., Anornu, G.K., 2022. Smart irrigation monitoring and control strategies for improving water use efficiency in precision agriculture: a review. Agric. Water Manag. 260, 107324.

Cabangon, R.J., Tuong, T., 2000. Management of cracked soils for water saving during land preparation for rice cultivation. Soil Tillage Res. 56, 105–116.

Callaghan, M.V., Head, F.A., Cey, E.E., Bentley, L.R., 2017. Salt leaching in fine-grained, macroporous soil: negative effects of excessive matrix saturation. Agric. Water Manag. 181, 73–84.

Cassiani, G., Boaga, J., Vanella, D., Perri, M.T., Consoli, S., 2015. Monitoring and modelling of soil–plant interactions: the joint use of ert, sap flow and eddy covariance data to characterize the volume of an orange tree root zone. Hydrol. Earth Syst. Sci. 19, 2213–2225.

Chartzoulakis, K., Bertaki, M., 2015. Sustainable water management in agriculture under climate change. Agricult. Agricult. Sci. Proced. 4, 88–98.

Ciani, L., Patrizi, G., Innocenti, A., Fanti, R., Pazzi, V., 2024. Considerations on the electrode spacing to electrode diameter ratio in electrical resistivity tomography (ert): an operational approach. IEEE Trans. Instrum. Meas. 73, 1–12. https://doi.org/10.1109/TIM.2024.3375950. Art no. 4504312.

Cordero-Vázquez, C.Y., Delgado-Rodríguez, O., Cisneros-Almazán, R., Peinado-Guevara, H.J., 2023. Determination of soil physical properties and pre-sowing irrigation depth from electrical resistivity, moisture, and salinity measurements. Land 12, 877.

Dahlin, T., 2000. Short note on electrode charge-up effects in dc resistivity data acquisition using multi-electrode arrays. Geophys. Prospect. 48, 181–187.

De Carlo, L., Battilani, A., Solimando, D., Caputo, M.C., 2020. Application of time-lapse ert to determine the impact of using brackish wastewater for maize irrigation. J. Hydrol. 582, 124465.

Gao, H., Yan, C., Liu, Q., Ding, W., Chen, B., Li, Z., 2019. Effects of plastic mulching and plastic residue on agricultural production: a meta-analysis. Sci. Total Environ. 651, 484–492.

Gu, Z., Qi, Z., Burghate, R., Yuan, S., Jiao, X., Xu, J., 2020. Irrigation scheduling approaches and applications: a review. J. Irrig. Drain. Eng. 146, 04020007.

Innocenti, A., Pazzi, V., Napoli, M., Fanti, R., Orlandini, S., 2024. Assessing the efficiency of the irrigation system in a horticulture field through time-lapse electrical resistivity tomography. Irrig. Sci. 1–15.

Inoue, H., 1993. Lateral water flow in a clayey agricultural field with cracks. Geoderma 59, 311–325.

Jia, J., Zhang, P., Yang, X., Zhen, Q., Zhang, X., 2021. Comparison of the accuracy of two soil moisture sensors and calibration models for different soil types on the loess plateau. Soil Use Manag. 37, 584–594.

Karaoulis, M., Tsourlos, P., Kim, J.H., Revil, A., 2014. 4d time-lapse ert inversion: introducing combined time and space constraints. Near Surf. Geophys. 12, 25–34.

Li, J., Li, L., Chen, R., Li, D., 2016. Cracking and vertical preferential flow through landfill clay liners. Eng. Geol. 206, 33–41.

Li, F., Tan, C., Dong, F., 2020. Electrical resistance tomography image reconstruction with densely connected convolutional neural network. IEEE Trans. Instrum. Meas. 70, 1–11.

Li, C., Luo, X., Li, Y., Wang, N., Zhang, T., Feng, H., Zhang, W., Siddique, K.H., et al., 2023. Ridge planting with transparent plastic mulching improves maize productivity by regulating the distribution and utilization of soil water, heat, and canopy radiation in arid irrigation area. Agric. Water Manag. 280, 108230.

Light, T.S., Licht, S., Bevilacqua, A.C., Morash, K.R., 2004. The fundamental conductivity and resistivity of water. Electrochem. Solid-State Lett. 8, E16.

Liu, P., Wang, H., Li, L., Liu, X., Qian, R., Wang, J., Yan, X., Cai, T., Zhang, P., Jia, Z., et al., 2020. Ridge-furrow mulching system regulates hydrothermal conditions to promote maize yield and efficient water use in rainfed farming area. Agric. Water Manag. 232, 106041.

Liu, X., Liu, W., Tang, Q., Liu, B., Wada, Y., Yang, H., 2022. Global agricultural water scarcity assessment incorporating blue and green water availability under future climate change. Earth's Future 10 e2021EF002567.

Loke, M., 2004. Tutorial: 2-D and 3-D Electrical Imaging Surveys.

Luo, X., Li, C., Lin, N., Wang, N., Chu, X., Feng, H., Chen, H., 2023. Plastic film-mulched ridges and straw-mulched furrows increase soil carbon sequestration and net ecosystem economic benefit in a wheat-maize rotation. Agric. Ecosyst. Environ. 344, 108311.

Mantel, S., Dondeyne, S., Deckers, S., 2023. World reference base for soil resources (wrb). Goss. In: Michael, J. (Ed.), Margaret Oliver Encyclopedia of Soils in the Environment, 2nd ed., pp. 206–217.

Mary, B., Vanella, D., Consoli, S., Cassiani, G., 2019. Assessing the extent of citrus trees root apparatus under deficit irrigation via multi-method geo-electrical imaging. Sci. Rep. 9, 9913.

Ochs, J., Klitzsch, N., 2020. Considerations regarding small-scale surface and borehole-to-surface electrical resistivity tomography. J. Appl. Geophys. 172, 103862.

Patrizi, G., Guidi, G., Ciani, L., Catelani, M., Cappuccini, L., Innocenti, A., Casagli, N., Pazzi, V., 2022. Analysis of non-ideal remote pole in electrical resistivity tomography for subsurface surveys. In: 2022 IEEE International Instrumentation and Measurement Technology Conference (I2MTC). IEEE, pp. 1–5.

Pazzi, V., Di Filippo, M., Di Nezza, M., Carlà, T., Bardi, F., Marini, F., Fontanelli, K., Intrieri, E., Fanti, R., 2018. Integrated geophysical survey in a sinkhole-prone area: Microgravity, electrical resistivity tomographies, and seismic noise measurements to delimit its extension. Eng. Geol. 243, 282–293.

Pereira, L., Paredes, P., Jovanovic, N., 2020. Soil water balance models for determining crop water and irrigation requirements and irrigation scheduling focusing on the fao56 method and the dual kc approach. Agric. Water Manag. 241, 106357.

Ratke, R.F., Zuffo, A.M., Steiner, F., Aguilera, J.G., de Godoy, M.L., Gava, R., de Oliveira, J.T., Filho, T.A.D.S., Viana, P.R.N., Ratke, L.P.T., et al., 2023. Can soil moisture and crop production be influenced by different cropping systems? AgriEngineering 5, 112–126.

Santarato, G., Ranieri, G., Occhi, M., Morelli, G., Fischanger, F., Gualerzi, D., 2011. Three-dimensional electrical resistivity tomography to control the injection of expanding resins for the treatment and stabilization of foundation soils. Eng. Geol. 119, 18–30.

Shi, K., Lu, T., Zheng, W., Zhang, X., Zhangzhong, L., 2022. A review of the category, mechanism, and controlling methods of chemical clogging in drip irrigation system. Agriculture 12, 202.

Technologies, S.E., 2001. Calibration of the Sentek Pty Ltd Soil Moisture Sensors.

Vanella, D., Cassiani, G., Busato, L., Boaga, J., Barbagallo, S., Binley, A., Consoli, S., 2018. Use of small scale electrical resistivity tomography to identify soil-root interactions during deficit irrigation. J. Hydrol. 556, 310–324.

Vanella, D., Ramírez-Cuesta, J.M., Sacco, A., Longo-Minnolo, G., Cirelli, G.L., Consoli, S., 2021. Electrical resistivity imaging for monitoring soil water motion patterns under different drip irrigation scenarios. Irrig. Sci. 39, 145–157.

Vanella, D., Peddinti, S.R., Kisekka, I., 2022. Unravelling soil water dynamics in almond orchards characterized by soil-heterogeneity using electrical resistivity tomography. Agric. Water Manag. 269, 107652.

Verdet, C., Anguy, Y., Sirieix, C., Clément, R., Gaborieau, C., 2018. On the effect of electrode finiteness in small-scale electrical resistivity imaging. Geophysics 83. EN39–EN52.

Viero, A., Galgaro, A., Morelli, G., Breda, A., Francese, R., 2015. Investigations on the structural setting of a landslide-prone slope by means of three-dimensional electrical resistivity tomography. Nat. Hazards 78, 1369–1385.

Wang, X.L., Li, F.M., Jia, Y., Shi, W.Q., 2005. Increasing potato yields with additional water and increased soil temperature. Agric. Water Manag. 78, 181–194.

Wang, C., Zhang, Z.Y., Fan, S.M., Mwiya, R., Xie, M.X., 2018. Effects of straw incorporation on desiccation cracking patterns and horizontal flow in cracked clay loam. Soil Tillage Res. 182, 130–143.

Wang, Q., Li, X., Zhao, C., Pei, L., Wan, S., 2023. Evaluation analysis of the saturated paste method for determining typical coastal saline soil salinity. Soil Tillage Res. 225, 105549.
Wanniarachchi, S., Sarukkalige, R., 2022. A review on evapotranspiration estimation in agricultural water management: past, present, and future. Hydrology 9, 123.
Zhang, H., Schroder, J., Pittman, J., Wang, J., Payton, M., 2005. Soil salinity using saturated paste and 1: 1 soil to water extracts. Soil Sci. Soc. Am. J. 69, 1146–1151.
Zhang, W., Dong, A., Liu, F., Niu, W., Siddique, K.H., 2022. Effect of film mulching on crop yield and water use efficiency in drip irrigation systems: a meta-analysis. Soil Tillage Res. 221, 105392.
Zhou, B., Dahlin, T., 2003. Properties and effects of measurement errors on 2d resistivity imaging surveying. Near Surf. Geophys. 1, 105–117.